ISSN: 2414-1895 DOI: 10.6919/ICJE.202608_12(8).0015

Defect Detection and Grain Size Evaluation based on Metallographic Images of Long Shafts

Jianhong Liu[1], Yue Wang[2], Xingxing Xu[2], You Zhou[1], Ning Liu[1], Tingting Hu[2], Haitao Hu[2], Qiang Liu[1, *]

[1] Chengdu Metcera Advanced Materials Co., Ltd., Chengdu 610100, China

[2] AECC Aviation Power Co., Ltd., Xi'an 710021, China

Abstract

Aiming at the difficulties in identifying tiny surface defects and automatic grain size evaluation of long shaft parts, this paper proposes an automatic detection and grading method based on robot visual guidance and adaptive image segmentation. The YOLOv8 algorithm is adopted to identify surface defects on long shafts, and the defect coordinates are mapped to the base coordinate system through the hand-eye calibration matrix with a positioning error within 0.9 mm, which guides the end effector to complete fixed-point grinding and etching. This paper focuses on developing an OpenCV-based grain size calculation algorithm: CLAHE contrast enhancement, adaptive Gaussian threshold segmentation and watershed algorithm are applied to metallographic images after etching to accurately separate adhered grains. Pseudo-boundary interferences are eliminated via contour morphological filtering, and the average grain area method is finally used to calculate and grade grain sizes. Experiments verify that the proposed system realizes integrated operations from defect localization to metallographic grading for long shafts, with a repeatability error of grain size grading less than 0.5 grades, satisfying the high-precision detection requirements of industrial sites.

Keywords

Long Shaft Inspection; YOLOv8; Grain Size Grading; Watershed Algorithm.

1. Introduction

As core components of mechanical transmission systems, the operational stability of shaft parts directly affects the safe operation of major equipment. Particularly for high-speed shaft components, external and material defects directly affect the service life and reliability of the mechanical equipment. During shaft manufacturing, heating temperatures exceeding the β-phase transformation point during forging or solution heat treatment can lead to abnormal β grain growth, excessively high-temperature holding times, and insufficient local deformation. These factors result in inadequate dynamic recrystallization and retention of the ingot's original microstructure. Although coarse original β grains undergo α-phase precipitation upon cooling, their grain boundary contours remain intact, resulting in a significant increase in the average grain area and a reduction in the grain size grade within the metallographic structure. This reduces the shaft's resistance to plastic deformation, creating a risk of brittle fracture during use and shortening its service life. Therefore, grain size testing of shafts is of particular importance.

Currently, research on the intelligent inspection of shaft-type parts primarily focuses on surface defect detection. Liu Weiwei et al. [1] improved YOLOv5 by introducing an attention mechanism and a repeated-weighting bidirectional feature fusion strategy, significantly enhancing detection accuracy; Liu Zihao et al. [2] developed an image acquisition system for tubular parts with adjustable focal

ISSN: 2414-1895 DOI: 10.6919/ICJE.202608_12(8).0015

length and optimized the feature extraction module of YOLOv8; Sun Yuan et al. [3] proposed the RB-YOLOv8 algorithm, which achieved simultaneous improvements in both speed and accuracy for crankshaft defect detection by adjusting the C2f module and the BiFPN architecture. However, surface inspection alone is insufficient to assess the internal quality of a part; metallographic grain size grading remains a critical step. Grain size and morphology are core factors that determine the strength, toughness, and in-service stability of polycrystalline materials. Traditional manual grading relies on comparisons with standard atlases, which suffer from drawbacks such as high subjectivity, poor reproducibility, and low efficiency. To address this, Wang et al. [4] explored deep learning-based grading methods, and Yang et al. [5] proposed a partitioned gradient segmentation algorithm to eliminate optical interference. The team at Jiangsu University has made outstanding contributions in this field: Zhu Jiandong et al. [6] developed an adaptive Mean Shift segmentation algorithm; Bao Jinyue et al. [7] constructed a national standard metallographic dataset and achieved a 95% grading accuracy by utilizing multi-scale feature fusion with FCNN and end-to-end cascaded architectures; and Zhang Qi et al. [8] balanced efficiency and accuracy by building a multi-class metallographic database and a multi-feature ensemble classifier.

Simultaneously, grain characterization techniques have undergone profound methodological transformations [9]. To address the issues of low manual efficiency and difficulty in standard implementation associated with the traditional intersection method, an automated algorithm based on topological skeletons was the first to achieve standardized execution of the intersection method and plane analysis under optical microscopy [10]. By combining machine learning with the CHAC algorithm, researchers overcame the challenge of grain boundary identification in high-throughput UO_2 images from in-situ TEM irradiation experiments [11]. To address the bottleneck of scarce data in the pure iron system, the latest research introduced a denoised diffusion probability model (DDPM) to generate synthetic data, and in combination with an improved U-Net network, achieved intelligent statistics on the total grain area and twin merging, greatly enhancing the objectivity of the characterization [12].

In summary, most existing studies are limited to single-dimensional surface defect detection or the independent development of grain size algorithms and lack full-process automated inspection for components. Therefore, this study proposes an integrated inspection solution for shaft-type components. By combining the improved depth detection algorithm with automatic control technology, the proposed scheme realizes a full-process closed-loop inspection, covering intelligent identification and localization of surface defects, automatic robotic targeted grinding and polishing, chemical etching, and automatic grain size grading of metallographic images based on machine vision. This study provides a new technical pathway for the intelligent manufacturing and quality control of high-end shaft-type components.

2. Experiments and Analysis

2.1 System Configuration

The proposed inspection system primarily comprises a clamping-and-rotation unit, 6-axis manipulator, vision imaging module (equipped with a 25 MP camera, lens, and quadruple-partitioned illumination source), bore inspection module, automated grinding head exchange module, and metallurgical microscope exchange module. A quick-change disc is mounted on the end-effector of the manipulator, enabling rapid switching between the grinding assembly and metallographic microscopy assembly. A schematic of the setup is shown in Figure 1.

ISSN: 2414-1895 DOI: 10.6919/ICJE.202608_12(8).0015

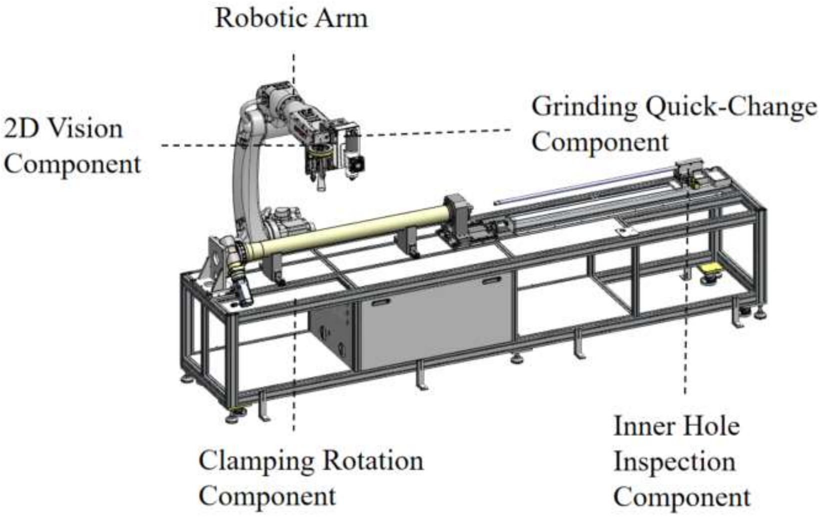

Figure 1. 3D Design drawing of the equipment

The overall workflow is as follows: The robotic arm grips the vision-imaging device, captures images of the shaft from left to right, and performs real-time detection and inference using the YOLOv8m model. Upon identifying a defect, the current robotic arm coordinates, rotation angle of the component, and pixel coordinates corresponding to the current position are recorded. After completing one round of inspection, the system rotates by 30 °and repeats the process until the entire outer surface of the shaft is inspected. Using the recorded defect locations, the grinding coordinates of the robot were calculated using the hand-eye calibration matrix. The robot is then controlled to move automatically to the grinding position for automated grinding. After grinding, the surface was etched, and the grinding quick-change assembly was replaced with a metallographic microscope. Upon receiving the trigger signal, the microscope moves above the defect location to capture metallographic images and perform grain size grading calculations. The flowchart is illustrated in Fig. 2. Owing to space constraints, this paper does not provide a detailed explanation of the inner-surface inspection.

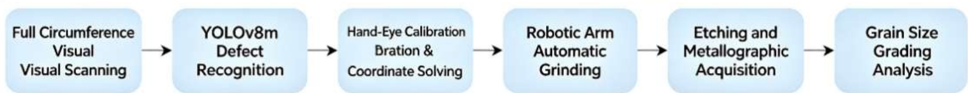

Figure 2. Equipment workflow diagram

2.2 Image Acquisition and Inference

Because defects are clearly visible only at specific illumination angles, the fixed illumination angles of commonly used ring lights and bar lights can easily lead to missed defects. To create varying illumination patterns, this study proposes the use of a four-zone light source with an illumination method that varies the brightness at different angles. For example, an illumination combination of (255, 50, 50, 50) emphasizes the brightness in one direction. Testing has shown that this approach is effective for detecting certain microscopic defects. As shown in Figure 3, different lighting combinations were applied to the same location.

ISSN: 2414-1895 DOI: 10.6919/ICJE.202608_12(8).0015

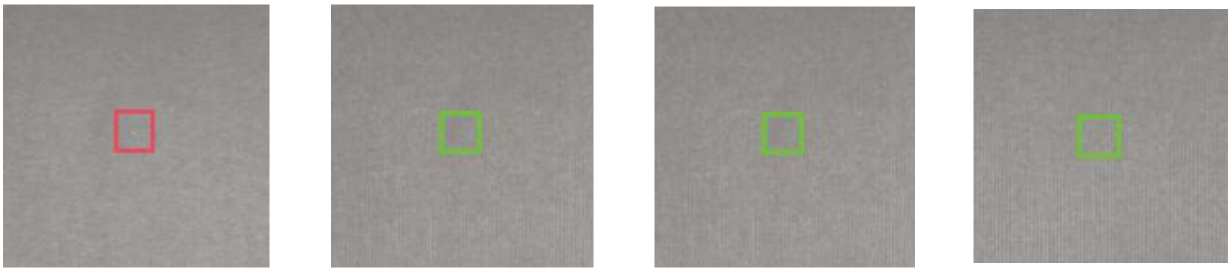

Figure 3. Local contrast comparison at the same position for a four-zone light source

As shown in the figure, at the same location, defects are visible only with one specific combination of light sources. The red box indicates the location where defects are visible, and the green box indicates the corresponding location where defects are not visible. Defect locations along multiple long axes were captured to build a defect dataset, which was annotated and used for training. The annotated defect images are shown below.

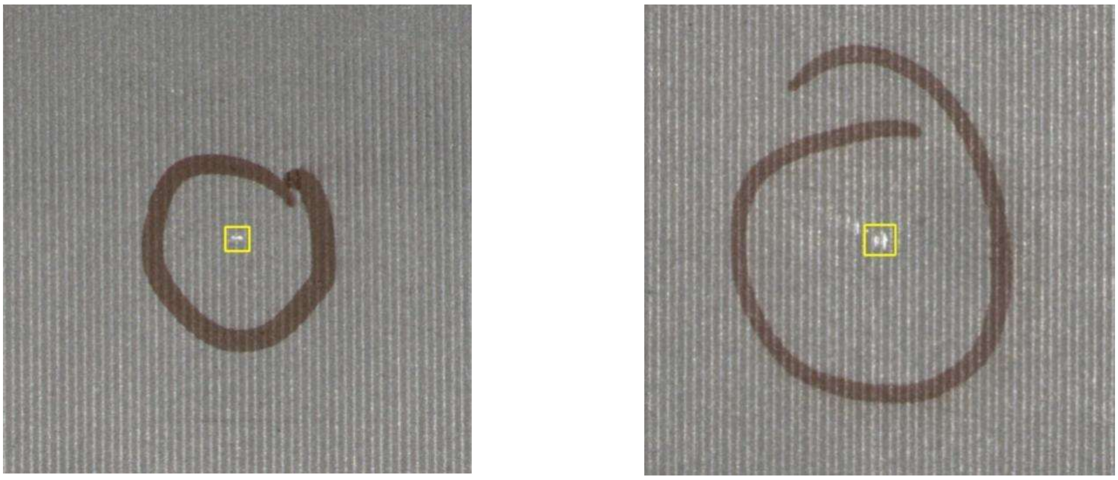

Figure 4. Defect annotations

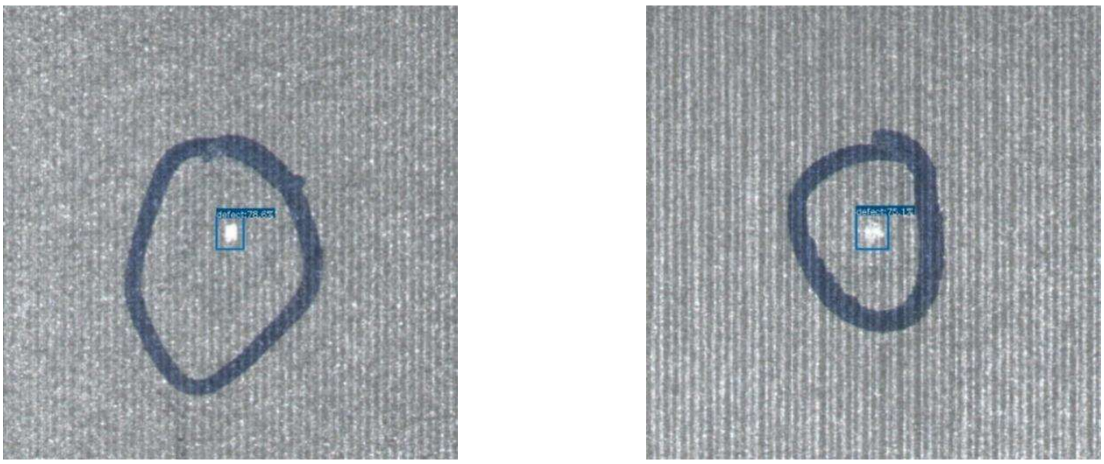

Figure 5. Inference results

The experiment utilized the YOLOv8m model, whose backbone network was based on CSPDarkNet and incorporated a C2f module to enhance the efficiency of extracting features related to segregation defects. Using over 200 annotated samples, the training was set to 500 iterations, and the SPPF

ISSN: 2414-1895 DOI: 10.6919/ICJE.202608_12(8).0015

module was used to enhance the multiscale feature fusion capabilities. After training was completed, an inference test was conducted on the validation set, and the inference results are shown in figure below.

2.3 Grinding and Corrosion

By integrating the inference results from the 2D surface inspection across the entire area, including the pixel coordinates of the defect locations, rotation axis angles, and the corresponding robotic arm coordinates, and combining them with the pre-calibrated hand-eye calibration matrix, the system performs rigid-body transformations and pose-matching calculations to map the defect coordinates from the pixel plane to the Cartesian space. Once the robotic arm moved to the polishing coordinates and orientation, it triggered an in-position signal to begin polishing, resulting in a smooth, mirror-like finish. An etching solution with a specific concentration was applied to the mirror surface, after which the system switched to the microscope and moved to the inspection position, as shown in the figure below.

(a)

(b)

Figure 6. a) Post-corrosion image, b) Metallographic microscope

2.4 Grain Size Analysis

2.4.1 CLAHE Contrast Enhancement

First, the captured RGB image was converted to a grayscale image. Owing to issues such as uneven brightness caused by corrosion, localized reflections, and grayscale variations at grain boundaries, a contrast-limiting mechanism was introduced to mitigate localized brightness anomalies caused by metal reflections. This mechanism suppresses noise amplification while preserving local details, thereby suppressing localized high-brightness areas and providing an image with clear features for further processing. The effect of increasing the local contrast is shown below.

(a)

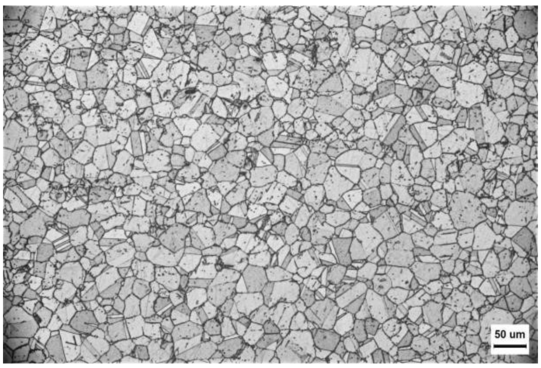

(b)

Figure 7. a) Original metallographic microscope image; b) CLAHE local contrast enhancement

ISSN: 2414-1895 DOI: 10.6919/ICJE.202608_12(8).0015

2.4.2 Adaptive Gaussian Threshold Segmentation

When performing threshold segmentation, a fixed threshold cannot adapt to the image characteristics of the gradually changing reflectance on corroded shaft-type surfaces, resulting in the complete loss of local grain details or large-area misclassification. We propose the use of a large-window Gaussian adaptive thresholding method for segmentation. A 255×255 large neighborhood window was used to perform Gaussian-weighted grayscale statistics, and a dynamic segmentation threshold was generated by subtracting a fixed offset from the window’s average grayscale value. This approach can be adapted to the overall brightness gradients across the entire image, ensuring the stability of grain boundary extraction.

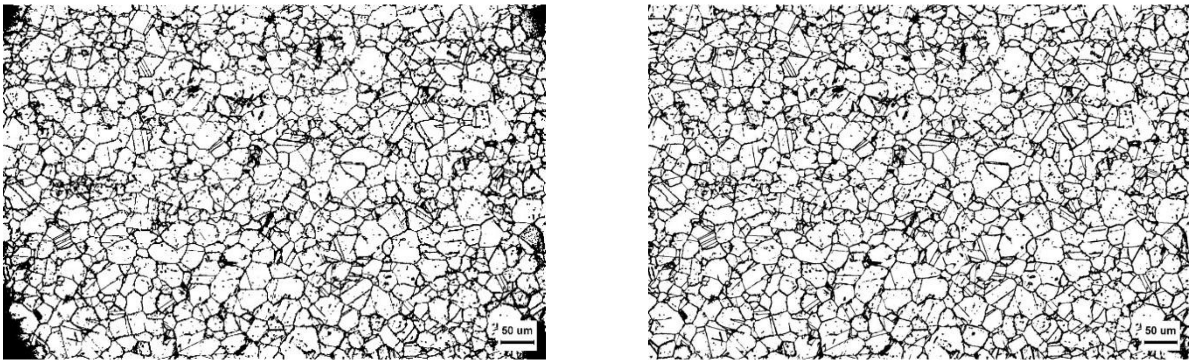

(a) (b)

Figure 8. a) Result of fixed thresholding; b) Result of Gaussian adaptive thresholding

As shown in the figure above, Gaussian weighting smooths excessive edge processing, resulting in fewer dark shadows and providing a clearer feature image for subsequent processing.

After adaptive Gaussian thresholding, although relatively clear contours are extracted, many small contours remain, which hinders subsequent segmentation and recognition. Based on the characteristics of these small contours, the contour areas in the image were statistically analyzed.

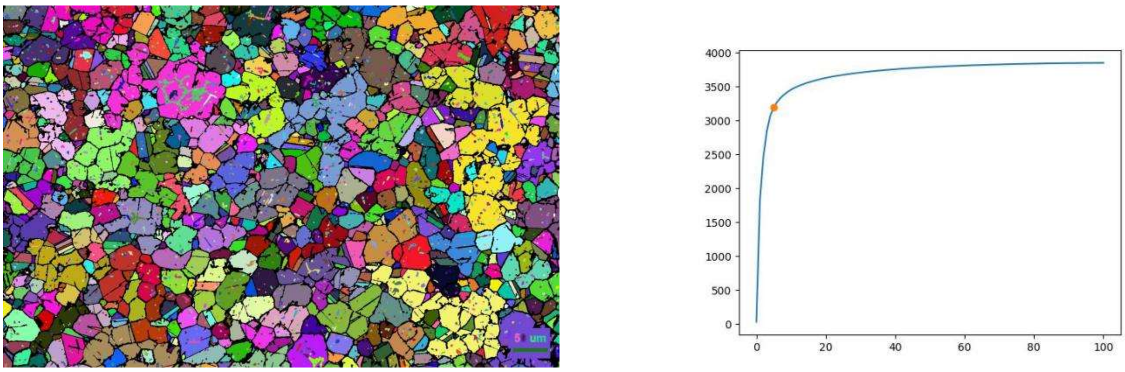

(a) (b)

Figure 9. a) Contour-colored segmentation; b) Relationship between contour area and number

In Figure (b), the horizontal axis represents the area percentage, and the vertical axis represents the number of contours. It can be seen that the vast majority of contours are small, accounting for approximately 5% of the total area. Contours that were numerous but had a small area were removed, as shown in the figure below.

ISSN: 2414-1895 DOI: 10.6919/ICJE.202608_12(8).0015

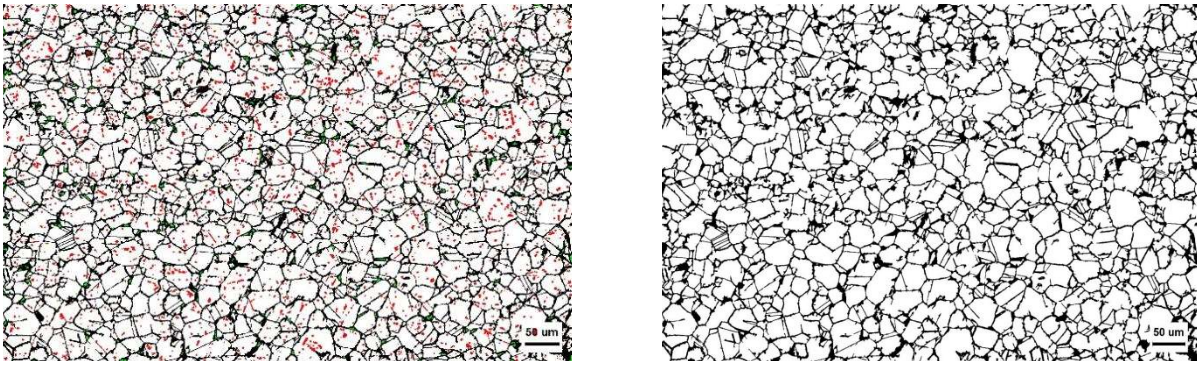

(a) (b)

Figure 10. a) Before small-feature removal, b) After small-feature removal

As shown in Figure (b), the outline is clearly visible, with no complex interference components.

2.4.3 Watershed Algorithm

After adaptive thresholding for coarse segmentation, a large number of adjacent grains tend to stick together at their boundaries and merge into clusters, making it impossible to count the grains individually, which is a core challenge in metallographic image analysis. We propose using a watershed segmentation algorithm to achieve a fine-grained separation of adhered grains. First, morphological opening and closing operations were applied to the binarized image to eliminate single-point corrosion noise and fill microscopic voids within the grains. Second, high-confidence foreground regions centered on the grain cores are extracted based on distance transform, and dilation is performed to identify pure background regions devoid of grains. Next, the regions where grains are fused together are marked as unknown areas awaiting segmentation, and a three-channel labeling matrix comprising foreground, background, and unknown regions is constructed and fed into the watershed model. Finally, based on the image's grayscale gradient, independent segmentation boundaries are automatically generated within the gaps between fused grains, ensuring that each grain forms a disjoint, independent region.

(a) (b)

Figure 11. a) Watershed results, b) Grain segmentation

After watershed segmentation, the image still contains false grain contours, such as erosion artifacts, scratch fragments, and invalid regions at the edges of the workpiece; direct counting would significantly reduce accuracy. This study proposes a multilayer contour filtering optimization mechanism to perform post-processing on post-watershed images and eliminate interference from false boundaries.

ISSN: 2414-1895 DOI: 10.6919/ICJE.202608_12(8).0015

2.4.4 Contour-Based Filtering to Eliminate False Boundary Interference

First, area threshold filtering is applied to remove noise fragments with excessively small pixel areas and excessively large invalid regions that fall outside the normal grain size range. Second, morphological feature screening is used to remove non-grain structures, such as elongated etching scratches and strip-shaped stains, based on contour roundness and aspect ratio. Next, morphological smoothing and repair are performed using a small-amplitude erosion-dilution operation to smooth jagged contours, repair broken grain boundaries, and ensure that grain contours are completely closed. Finally, duplicate fragments are merged, and small fragmented regions remaining after segmentation are fused to avoid errors caused by duplicate grain counting.

Map the processed contour back onto the original image. Simultaneously, to avoid distortion in the local contour calculations caused by incomplete boundary contours in the edge regions, the edge contours were removed (blue areas), and only the red areas were analyzed, as shown in the figure below.

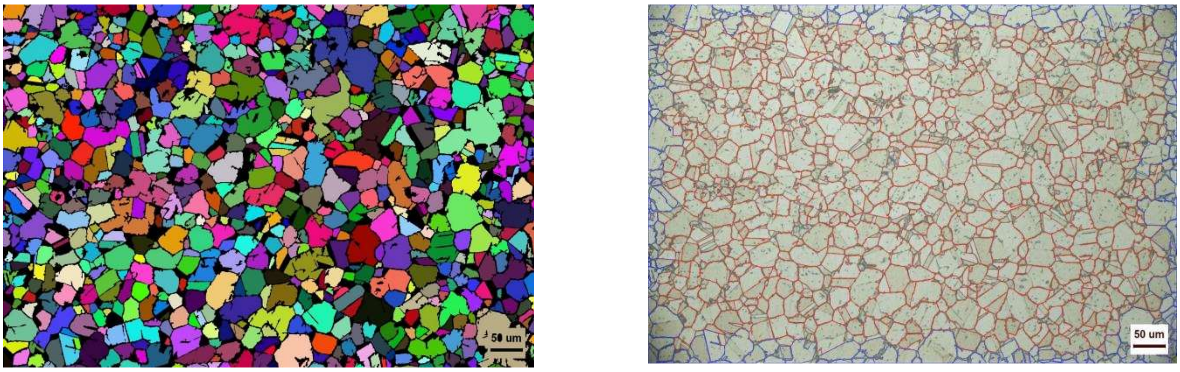

(a) (b)

Figure 12. a) Thresholding results, b) Post-processing after thresholding

2.4.5 Average Grain Area Method

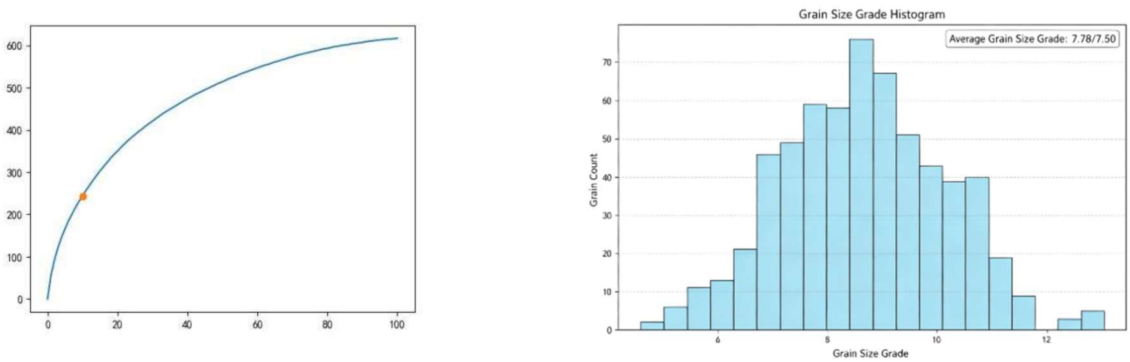

(a) (b)

Figure 13. a) Relationship between contour area and count; b) Histogram of grain size classes

This study introduces a standardized grain size calculation method based on the mean grain area. First, pixel-to-physical size calibration was performed. Relying on the calibrated parameters of the high-magnification metallographic objective, a conversion relationship between image pixels and the actual micrometer-scale dimensions was established, thereby eliminating dimensional errors caused by magnification variations. Next, global grain quantification was conducted. All screened, valid, and closed grain contours were traversed to count the total number of grains and accumulate the total

ISSN: 2414-1895 DOI: 10.6919/ICJE.202608_12(8).0015

physical area of the grains, from which the mean area per grain was calculated. Finally, conversion to the national standard grain size rating was carried out. Based on the mean grain area, the equivalent mean grain diameter and the mean intercept length were derived. These parameters were then substituted into the standard formula to automatically output the standardized grain size number.

As shown in the figure above, the average grain size grade calculated by the algorithm is 7.78, which differs by 0.28 from the grain size grade of 7.5 determined by manual inspection and meets the application requirements.

2.5 Verification of Algorithm Stability

To avoid the possibility that random fluctuations might cause the algorithm's results to appear as expected, we validated the results using several sets of images. The original images and corresponding grain size-specific histograms are shown in Table 1.

Table 1. Verification of algorithm stability

Original Image	Grain Size Distribution Histogram
	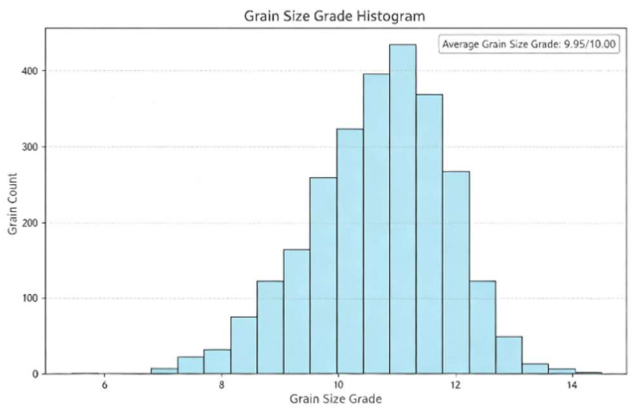
	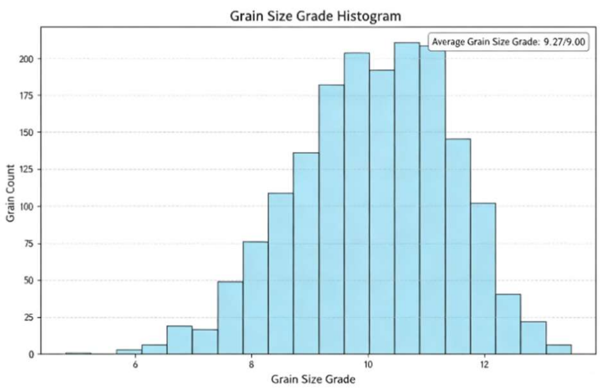

ISSN: 2414-1895 DOI: 10.6919/ICJE.202608_12(8).0015

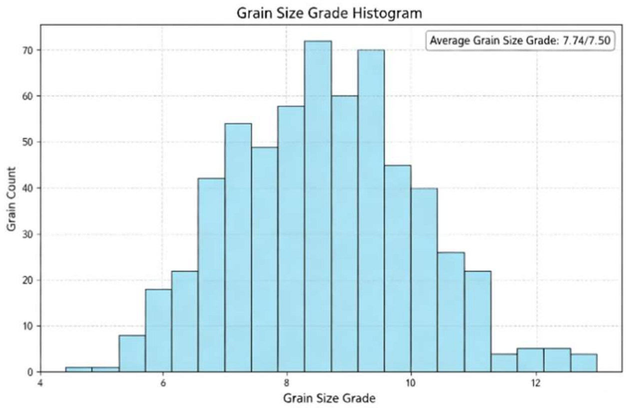

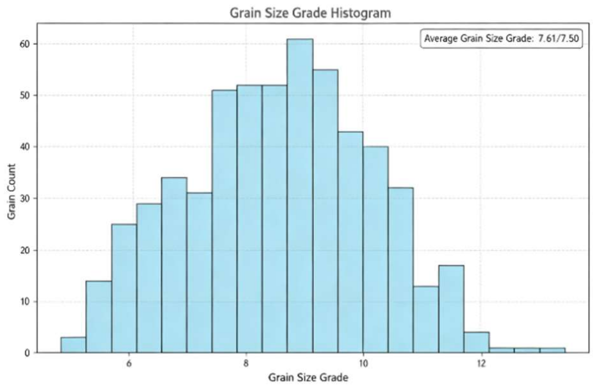

As shown in the table above, for images tested across two grain size grades, the discrepancy between the algorithm's detection results and the manual detection results was within 0.5 grade. This is consistent with the practical engineering applications.

2.6 Experimental Analysis

In summary, regarding the automated detection of surface defects on shafts and the grading of defect locations and grain size, this study focused on the severe issues of grain adhesion and boundary interference in corrosion metallographic images. This study proposes a high-precision grain size assessment algorithm based on OpenCV. By combining CLAHE contrast enhancement, adaptive Gaussian threshold segmentation, and the watershed algorithm, the algorithm achieves precise segmentation of the fused grains. Supplemented by contour morphological filtering to eliminate pseudo-boundary noise, the algorithm performs automatic grain size grading based on the average grain area method, effectively enhancing the intelligence and accuracy of the metallographic structure inspection. The algorithm's error margin relative to the manual calculations was within 0.5 grades.

3. Conclusion

This study addresses the engineering challenges of identifying minute surface defects on long-axis parts and the low accuracy of automated grain size assessment. We propose a method for the intelligent inspection and grain size grading of long-axis parts that integrates robot vision guidance with adaptive image segmentation. This study employed the YOLOv8 algorithm to detect surface defects in parts. By combining hand-eye calibration to map defect coordinates to a coordinate system, it controls the positioning errors to within 0.9 mm. The system can autonomously perform localized grinding and etching pretreatment on defects and process metallographic microscope images through contrast enhancement, adaptive threshold segmentation, the watershed algorithm, grain segmentation, denoising, and the area method to determine grain size grades. The detection accuracy differed from the manual inspection results by no more than 0.5 grades, meeting practical requirements. This

ISSN: 2414-1895 DOI: 10.6919/ICJE.202608_12(8).0015

effectively overcomes the shortcomings of traditional manual inspection, such as low accuracy, poor stability, and a high risk of missed or false detection.

References

[1] Liu, W. W., Qiu, J. H., Hu, G. D., et al. (2024). A method for detecting surface damage on decommissioned shaft components based on an improved YOLOv5. Journal of Northeastern University (Natural Science Edition), 45(07), 1002–1010.

[2] Liu, Z. H., Zhang, J. X., Xue, F., et al. (2025). A method for precise surface defect detection in pipe fittings based on an improved YOLO-v8. Journal of Zhejiang University. Engineering Edition, 59(7), 1514–1522, 1546.

[3] Sun, Y., Cao, J. J., Tang, J. Y., et al. (2024). An improved YOLOv8-based algorithm for crank shaft surface defect detection. Combined Machine Tools and Automated Machining Technology, (10), 77–81.

[4] Hu, H. J., Guo, R., & Zhang, Y. (2023). A deep learning-based method for grading the grain size of steel metallographic images. Optoelectronics and Lasers, 34(10), 1075.

[5] Song, Y., Su, R. C., & Wang, B. H. (2023). A method for extracting grain boundaries for automatic machine vision inspection of metal grain size. Metallurgical Automation, 47(S1), 320–326.

[6] Bao, J. Y. (2020). A study on automatic grain boundary segmentation and grading of metallographic images based on fully convolutional neural networks [Master’s thesis]. Jiangsu University. https://doi.org/10.27170/d.cnki.gjsuu.2020.001060

[7] Zhu, J. D. (2018). A study on algorithms for grain boundary extraction from metallographic images of steel and the design of intelligent grading software [Master’s thesis]. Jiangsu University.

[8] Zhang, Q. (2018). A study on an automatic metallographic structure grading method based on ensemble learning [Master’s thesis]. Jiangsu University.

[9] Banerjee, S., Chakraborti, P. C., & Saha, S. K. (2019). An automated methodology for grain segmentation and grain size measurement from optical micrographs. Measurement, 140, 142–150.

[10] Li X, Cui L, Li J, Chen Y., et al. (2022). Automation of intercept method for grain size measurement: A topological skeleton approach. Materials & Design, 224: 111358.

[11] Xu, X., Yu, Z., Chen, W. Y., et al. (2024). Automated analysis of grain morphology in TEM images using convolutional neural network with CHAC algorithm. Journal of Nuclear Materials, 588, 154813.

[12] Gao, Z., & Zhou, Y. (2025). Automated grain analysis via data augmentation and grain boundary detection. Micron, 103961.